High Cadence Radio Observations of an EIT Wave

S. M. White[1] and B. J. Thompson[2]

ABSTRACT

Sensitive radio observations of the 1997 September 24 EIT wave show its velocity to be 830 km s^{-1}. The wave first appears a short distance from the flare site, and its trajectory projects back to the flare site at the peak of the impulsive phase. The radio spectrum appears to be consistent with optically thin coronal emission rather than chromospheric emission. The observed radio brightness temperatures are consistent with the EIT fluxes if the temperature of the emitting gas is not at the peak formation temperature of the Fe XII 195 Å line, or if abundances are closer to photospheric than coronal. An important result is that no deceleration is observed during the 4 minutes that the wave is visible in the radio images: the discrepancy between EIT wave and Hα Moreton wave speeds requires that EIT waves slow substantially as they propagate, if they are the same disturbance.

Subject headings: Sun: flares – Sun: corona – Sun: radio radiation

1. INTRODUCTION

The so-called "EIT waves", also known as "coronal Moreton waves", are disturbances seen to propagate outwards from flare locations in EUV images of flares. They acquired their colloquial name when detected in coronal lines at EUV wavelengths by the Extreme-ultraviolet Imaging Telescope (EIT) on the SOHO satellite (Thompson et al. 1998, 1999), although the first detection of this class of events may have been obtained by Neupert (1989). The current name remains popular at present while the relationship of these phenomena to the other types of propagating disturbances associated with these events (e.g., Hα Moreton waves in the chromosphere, coronal mass ejections, "coronal dimmings" and the shock waves that produce Type II radio bursts; Klassen et al. 2000; Biesecker et al. 2002) is clarified. We use the term "EIT wave" here for brevity.

---

[1]Astronomy Department, University of Maryland, College Park, MD 20742; whiteastro.umd.edu

[2]NASA/Goddard Space Flight Center, Greenbelt, MD, 20771; barbara.thompsongsfc.nasa.gov

The disturbances were first recognized in sequences of EIT Fe XII 195 Å images obtained with a cadence of 7 to 23 minutes. The 195 Å images represent emission by plasma at around 1.5 $\times 10^6$ K, i.e., a typical quiet-coronal temperature. Thompson et al. (2000) discuss one of the most striking examples of this phenomenon, from 1997 September 24, in which a particularly sharp front propagates away from a flare site. This event also illustrates the incompleteness of the EIT coverage of a typical event: the wave front is clearly seen as a sharp feature in only one image (it is much more diffuse and amorphous in two subsequent frames) and the propagation speed therefore cannot easily be measured from the EIT data. In other events where the speeds can be measured (i.e., when a common wave feature can be clearly identified in two or more images), values of typically 200 - 400 km s^{-1} are found, but this range is subject to a strong selection effect: fast EIT waves cannot have their speeds measured because they propagate too far between EIT images to be detected at two locations. The early development of these events cannot be studied from images with a low cadence because they cannot easily be identified: in particular, an important question is whether the wave is launched by the impulsive phase of the flare, or does it arise in association with, e.g., a coronal mass ejection (CME) following the flare?

The relationships between propagating phenomena associated with flares remain poorly understood. Warmuth et al. (2004a) have presented a compelling case that Moreton waves and EIT waves represent the edge in the chromosphere and low corona, respectively, of a freely propagating fast–mode shock as it expands outwards, and that the shocks that produce Type II radio bursts are driven at the upper coronal edge of this wave. Whether the wave itself is driven by a CME remains an open question. Propagating fronts similar to EIT waves can also be seen in soft X-ray images (Khan & Aurass 2002; Narukage et al. 2002a; Hudson et al. 2003). Gilbert et al. (2004) observe waves as dark features in He I 10830 Å images that appear cospatial with the corresponding EIT waves: they argue that the chromospheric response is the "ground track" of the coronal disturbance as originally proposed by Uchida (1968). In several cases where Hα observations of a Moreton wave and EIT detections of a wave are both available, the data are consistent with them being coincident (Thompson et al. 2000; Pohjolainen et al. 2001; Warmuth et al. 2001). A clear requirement for the identification of EIT waves with Moreton waves would seem to be that they should have the same velocity. There are a number of events where this does not seem to be the case (Eto et al. 2002; Narukage et al. 2002b), but Warmuth et al. (2001) and Warmuth et al. (2004a) argue that this is due to deceleration of the wave front over time.

EIT waves are particularly difficult to observe, which is why they were not recognized until more than 25 years after the other forms of disturbance. Here we show that radio techniques can also produce images of EIT waves, and that the high cadence of the radio data provides information difficult to obtain with limited cadence or limited field of view EUV observations. Radio emission from these waves is weak and difficult to detect. Apart from this event (White & Thompson 2002), only two other studies have reported radio detections of this phenomenon: Aurass et al. (2002)

report a radio feature moving in the same direction as an EIT wave but not coincident with it, and Warmuth et al. (2004a) detect emission from a feature moving with an Hα Moreton wave that unfortunately occurred while EIT was unavailable.

2. Radio Observations of the 1997 September 24 Event

We report Nobeyama Radioheliograph (NoRH) observations at 17 and 34 GHz of the 1997 September 24 EIT wave event studied in detail by Thompson et al. (2000) and Warmuth et al. (2004a). This was associated with a GOES class M5.9 flare, and it is recognized as one of the few EIT wave events in which the data show a sharp front (Biesecker et al. 2002). The event was accompanied by an Hα Moreton wave with a speed of order 500 km s^{-1}, whose position is apparently consistent with that of the EIT wave at the time of the sharp front. In order to achive the high dynamic range necessary to detect radio emission from this feature against the strong nonthermal radio emission from the main flare site, the NoRH data were analyzed using the AIPS package which allows the use of self–calibration techniques. A sequence of NoRH 17 GHz radio images of the event typically 30 s apart is shown in Figure 1. The main flare site is at the bottom of each panel and consists of two sources some $100''$ apart (the overexposed dark regions) lying over sunspots at the trailing (brightest source) and leading ends of the active region. The fact that nonthermal electrons are seen over such a wide distance indicates that the flare involved large-scale magnetic loops.

There is no sign of the EIT wave in the radio images prior to 02:49:00 UT, and subsequently it develops initially as an enhancement to the north and northwest of the main flare source (within 5 s of 02:49:08 in Figure 1). We note that some emission features along a position angle at about $10°$ west of the north direction from the main flare source are artefacts because the point-response function was susceptible to errors along this direction. The subsequent radio images show the EIT wave moving predominantly northwards in the form of an irregular arc of emission; in the early stages the emission is brightest in the northwest direction, but later it is brightest to the north as in the EIT image. The evolution appears to be very similar to that seen in the Hα data of Thompson et al. (2000). Features identified with the EIT wave can be seen in the 17 GHz radio images at least until 02:53 UT. The peak brightness temperature in the EIT wave features is initially close to 5000 K (above the background disk emission level of 10^4 K) and decreases to 1000 K as it fades.

The exact timing of the EIT images is uncertain by up to 2 minutes due to a drifting on–board clock. The nominal corrected time of the image containing the sharp wave is 02:49:21 UT: at this time the radio feature is significantly south of the EIT feature, and does not show as complete an arc as in later images. The radio wave is identical to the EIT wave in position and shape in the time range within 10 s of 02:51:00, corresponding to the original clock time of the image (02:51:10 UT).

Given the similarity in shape and position between the EIT wave and the radio wave at 02:51:00 UT, we argue that the simplest assumption is that they are coincident at this point and this sets the time of the EIT image. At this time the signal strength in the sharp EIT wave is of order 300 DN/pixel/s: assuming a temperature of order 1.5×10^6 K, close to the formation temperature of the Fe XII Å line, the routine `eit_flux` in the EIT calibration software in the *SOLARSOFT* package yields an emission measure of order 8×10^{26} cm^{-5} (assuming Mazzotta et al 1998 ionization equilibrium and coronal abundances). The brightness temperature contribution expected from this material due to thermal bremsstrahlung is 450 K (Dulk 1985). This is much less than the observed radio brightness temperature of order 2500 K at 02:51:10. However, since the EIT wave is only observed with a single EIT bandpass we cannot derive a temperature for the EUV–emitting gas and so the value for the temperature must be assumed: if the true temperature is 1.0×10^6 K, then the emission measure would be 1.3×10^{27} cm^{-5} and the radio brightness temperature contribution would be 900 K. If the true temperature is 2.0×10^6 K, the emission measure would be 3.4×10^{27} cm^{-5} and the brightness temperature would be 1700 K. The abundance of the EUV–emitting gas is also an issue: if photospheric rather than coronal abundances are assumed, then because the Fe/H abundance is about a factor of 4 smaller, the inferred emission measure is about a factor of 4 larger and so are the expected radio brightness temperatures, bringing them closer to the observed values. Hudson et al. (2003) have estimated a smaller but comparable emission measure of 5×10^{26} cm^{-5} at a temperature 2.5×10^6 K for a wave front seen in Yohkoh/SXT soft X–ray data.

The radio images show the sharp front for a period of 4 minutes, during which time the wave moves about $300''$. Figure 2 shows the position of the wave front (the centroid) measured due north from the main flare site (the eastern radio peak in Figure 1 at about -340$''$, -560$''$), as well as the 17 GHz radio light curve. A fit to the measured positions gives a speed of order 835 km s^{-1}, and the positions project back to the flare site at the time of onset of the impulsive phase. The patchy nature of the radio emission associated with the wave makes it difficult to determine speeds along many different directions, but the nearly circular shape of the wave front suggests that the speed of the section due north of the flare site is roughly appropriate for most of the propagating front. The radio velocity is somewhat larger than the speed of the Hα Moreton wave, determined by Thompson et al. (2000) and Warmuth et al. (2004a) to be about 500 km s^{-1}, and the onset time we infer for the wave is correspondingly later than the estimate of 02:43 UT made by Thompson et al. (2000) on the basis of the Hα data. However, Thompson et al. (2000) state that the times of the Hα images are uncertain by of order 30 seconds, giving a positional uncertainty of about 40$''$ at the speed of the wave, and a detailed comparison of the Hα data with the radio data is therefore difficult.

3.   DISCUSSION

We believe that the EIT–wave radio emission is produced by thermal free-free emission (i.e., bremsstrahlung) from material swept up or otherwise disturbed by the wave. Brightness temperatures of order 3000 – 5000 K as observed for this EIT wave can in principle be due either to optically thick chromospheric emission (i.e., the wave causes the chromosphere to become optically thick further up the temperature gradient than is normal for 17 GHz) or to optically thin coronal emission. The correlation with the coronal Fe XII EUV emission argues for the latter interpretation, and a discriminant between these two possibilities would be provided by the radio flux spectrum, which is flat for optically thin emission but rising with frequency–squared for optically thick emission. However, the EIT wave is just barely visible in NoRH 34 GHz images, which are less sensitive than the 17 GHz images: the typical rms noise level while the EIT wave is visible is 2400 K. The radio spectrum is therefore poorly constrained, but it seems to be more consistent with the flat flux spectrum expected for optically thin thermal free-free emission (expected 34 GHz brightness temperature contribution of order 1000 K) than with the increasing flux spectrum of optically thick chromospheric emission (brightness temperature of order 4000 K over the area of the wave). We note that optically–thin thermal free-free emission does not have a very strong temperature dependence ($\propto T^{-0.5}$), so bright features can reliably be ascribed to density enhancements, not temperature effects: in fact, a temperature increase due to heating would result in a radio flux decrease if the density does not change. We can therefore rule out temperature changes as a significant factor in the detectability of these waves, and both the EUV emission and the radio emission in this event most likely arise from a density increase in the low corona. This further implies that if the EIT wave is a propagating wave, then it must be compressional in order to produce a density increase. We find that the radio brightness temperature declines with time as it propagates, consistent with Warmuth et al. (2004b)'s argument that the amplitude of the disturbance is decreasing. One might expect that a CME–driven disturbance would not show this behaviour because the momentum of the CME is so large that it can absorb the swept–up material without slowing: in that case the amount of material swept up and compressed by the shock increases with time, which would produce increasing radio emission. The lack of radio emission prior to 02:49:00 could arise because the thickness of the compressed region is small, or because the compression prior to that time takes place at heights where the initial density is so low that the compressed material is not visible in the radio images, but more examples are needed to understand the onset of the radio emission.

In our measurements the EIT wave shows no deceleration over the almost 5 minutes that it is visible in the radio images, to within the uncertainty in the data. It is crucial for the argument that coronal EIT waves and chromospheric Hα Moreton waves coincide that in cases where their speeds differ, deceleration of the wave over time be a viable explanation for the generally slower

speeds of the EIT waves. Warmuth et al. (2004a) show the velocity behaviour of 11 Hα Moreton waves and all appear to display a decrease in velocity, with the largest change occurring in the first 200 s of observations. Warmuth et al. (2004b) show that deceleration is observed at all wavelengths where disturbances are detected. Since Hα Moreton waves are typically observed only close to the flare, whereas the EIT waves can be observed more than a solar radius from the initiation point, a disturbance that starts out fast and rapidly slows would allow us to reconcile the differing Hα and EUV speeds. The event shown here does not fit this pattern: we measure a steady speed of around 800 km s^{-1} in the radio data for up to 300 s from flare onset, while Thompson et al. (2000) derive a speed of 500 km s^{-1} for the Hα Moreton wave between 02:47 and 02:50 UT. If the times of the Hα images are indeed correct to within 30 s of the nominal times, then the Hα Moreton wave appears even before the onset of the radio wave, but interestingly it appears first at exactly the location to the north–west of the main flare site where the radio wave is first seen (see Fig. 5 of Thompson et al. 2000). Errors of order 3 minutes in the times of the Hα images would be needed if the radio wave is colocated with the Hα wave.

The high speed of the EIT wave in this event is inconsistent with the simulations of fast–mode MHD waves by Wang (2000), in which the wave is initiated at a height of 35,000 km and is found to refract into regions of low Alfvén speed, i.e., away from active regions and coronal holes, and towards greater height. Because of the low Alfvén speed over the quiet Sun, the simulated disturbance is observed to have a speed down around 200 km s^{-1} in the corona. Chen et al. (2002) also carry out simulations of EIT waves and they argue that the fast coronal Moreton waves and the slow EIT waves are different disturbances that both arise naturally out of their scenario: their results are not consistent with the observations of this event since at no stage is the EIT wave behind the radio or the Hα Moreton wave as they predict.

One drawback to the MHD wave model is that, since coronal material is compressed in place and not transported by the wave, it does not by itself explain the "coronal dimmings" that appear in EIT images behind the EIT wave front (Zarro et al. 1999). In this event, at 02:51:10 UT the dimming of 195 Å emission behind the front (visible in the bottom panel of Fig. 1 as the bright area north and north–east of the plus symbol) is almost as dark (250 DN/pixel/s) as the front is bright (300 DN/pixel/s). If it is a density depression then it should be almost as prominent in radio difference images. There is a suggestion of a faint radio dimming coincident with the EUV dimming in this event, but it is not as striking as the appearance of the emission front.

4.   CONCLUSIONS

High dynamic range radio observations of the 1997 September 24 EIT wave allow us to measure the speed of the wave at 830 km s^{-1}: this is much faster than the normal range of measured

EIT wave speeds. We argue that this confirms the belief that the cadence of EIT observations is responsible for the typical low speeds (200 - 400 km s^{-1}) recorded for EIT waves: EIT itself usually cannot measure the speed of faster disturbances due to limits on its cadence. The radio data indicate that the wave first appears at some distance from the flare site. The initial feature is not very broad in position angle, and subsequently spreads laterally. The position of the EIT wave projects back to the flare site at the time of the peak of the impulsive phase: further work is needed to decide whether this is still consistent with a link between the EIT wave and the CME. Since the radio data are sensitive to density enhancements rather than temperature changes, they confirm that the wave phenomenon observed by EIT is not a temperature effect. The brightness temperature of the radio emission is consistent with the signal in the EIT image if the temperature of the emitting gas is significantly different from 1.5×10^6 K, or if the abundance of low first ionization potential elements such as Fe is low (closer to photospheric rather than coronal values).

No deceleration of the wave is observed while it is visible in the radio images. The issue of deceleration is critical since it is required to explain why the EIT–observed waves have much slower speeds than the Hα Moreton waves in the same events, if they are due to the same disturbance, and clearly further studies of this question in other events are needed.

REFERENCES

Aurass, H., Shibasaki, K., Reiner, M., & Karlický, M. 2002, Astrophys. J., 567, 610

Biesecker, D. A., Myers, D. C., Thompson, B. J., Hammer, D. M., & Vourlidas, A. 2002, Astrophys. J., 569, 1009

Chen, P. F., Wu, S. T., Shibata, K., & Fang, C. 2002, Astrophys. J. (Lett.), 572, L99

Dulk, G. A. 1985, Ann. Rev. Astron. Astrophys., 23, 169

Eto, S., et al. 2002, Publ. Astron. Soc. Japan, 54, 481

Gilbert, H. R., Holzer, T. E., Thompson, B. J., & Burkepile, J. T. 2004, Astrophys. J., 607, 540

Hudson, H. S., Khan, J. I., Lemen, J. R., Nitta, N. V., & Uchida, Y. 2003, Solar Phys., 212, 121

Khan, J. I. & Aurass, H. 2002, Astron. Astrophys., 383, 1018

Klassen, A., Aurass, H., Mann, G., & Thompson, B. J. 2000, Astron. Astrophys. Supp. Ser., 141, 357

Mazzotta, P., Mazzitelli, G., Colafrancesco, S., & Vittorio, N. 1998, Astron. Astrophys. Supp. Ser., 133, 403

Narukage, N., Hudson, H. S., Morimoto, T., Akiyama, S., Kitai, R., Kurokawa, H., & Shibata, K. 2002a, Astrophys. J. (Lett.), 572, L109

Narukage, N., Morimoto, T., Kitai, R., Kurokawa, H., & Shibata, K. 2002b, in 8th Asian-Pacific Regional Meeting, Volume II, 449–450

Neupert, W. M. 1989, Astrophys. J., 344, 504

Pohjolainen, S., et al. 2001, Astrophys. J., 556, 421

Thompson, B. J., et al. 1999, Astrophys. J. (Lett.), 517, L151

Thompson, B. J., Plunkett, S. P., Gurman, J. B., Newmark, J. S., St. Cyr, O. C., & Michels, D. J. 1998, Geophys. Res. Lett., 25, 2465

Thompson, B. J., et al. 2000, Solar Phys., 193, 161

Uchida, Y. 1968, Solar Phys., 4, 30

Wang, Y.-M. 2000, Astrophys. J. (Lett.), 543, L89

Warmuth, A., Vršnak, B., Magdalenić, J., Hanslmeier, A., & Otruba, W. 2004a, Astron. Astrophys., 418, 1101

—. 2004b, Astron. Astrophys., 418, 1117

Warmuth, A., Vršnak, B., Aurass, H., & Hanslmeier, A. 2001, Astrophys. J. (Lett.), 560, L105

White, S. M. & Thompson, B. J. 2002, Bulletin of the American Astronomical Society, 34, 681

Zarro, D. M., Sterling, A. C., Thompson, B. J., Hudson, H. S., & Nitta, N. 1999, Astrophys. J. (Lett.), 520, L139

Fig. 1.— NoRH 17 GHz observations of the propagating disturbance on 1997 September 24. Panels show contours of the images (after preflare subtraction) plotted over difference images (the image 30 s earlier is subtracted from the image at the time indicated) in reversed greyscale (bright features appear dark). Contours are at brightness temperature multiples of 600 K up to 7200 K (the disk component of 10000 K has been subtracted before plotting), and the top three contours are at 0.365, 1.96 & 4.85 × 10^6 K. The images have a pixel size of 3″ and have been convolved with a 33″ gaussian to enhance large-scale features. For comparison, the last panel shows the EIT difference image at 02:49:21. The plus symbol in the last two panels shows the center of a circle fit to the EIT wave front in the bottom panel.
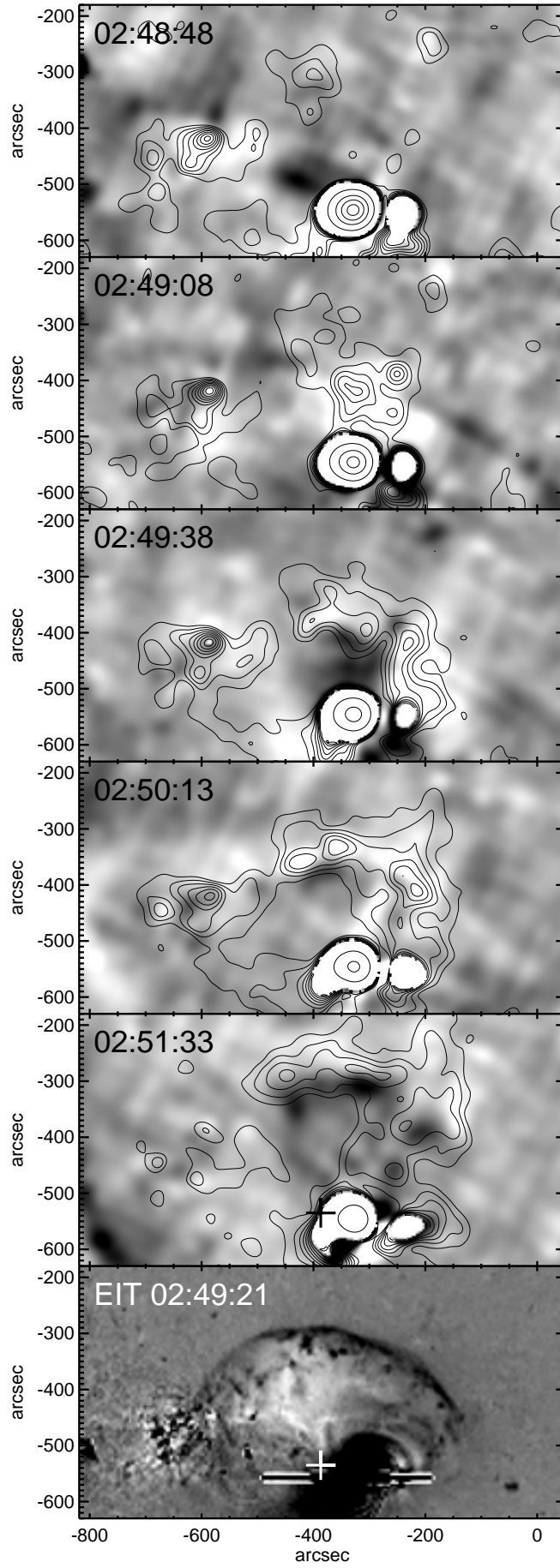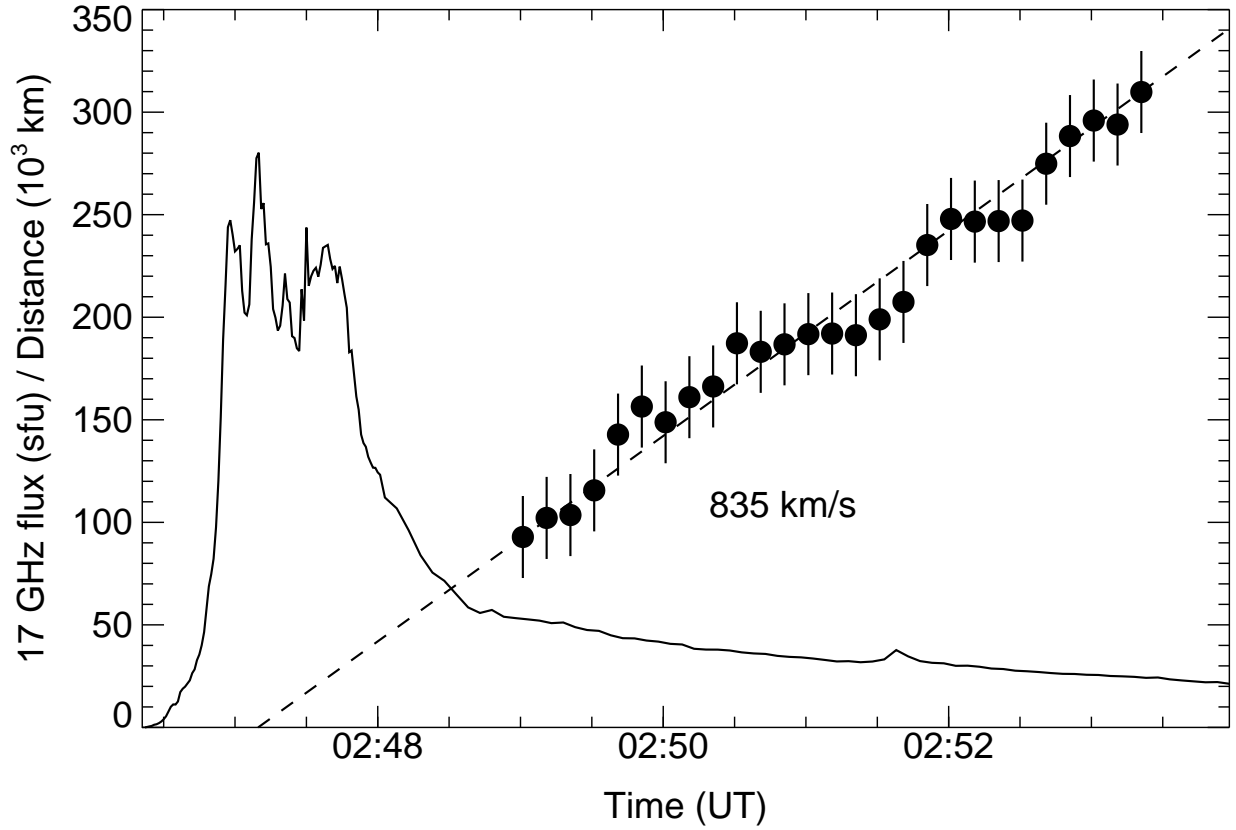
Fig. 2.— The 17 GHz time profile of the flare (solid line) together with the observed distance of the EIT wave from the flare location (in 10^3 km) at the position angle due north of the main flare site (dots with error bars), and a dashed line representing a constant velocity of 835 km s^{-1}. The radio flux measurements are taken from images made every second during the impulsive phase and every 5 s after 02:48 UT.